

Wrinkling deformation and thermal conductivity of one graphane sheet under shear

Haijun Shen

School of Aerospace Engineering and Applied Mechanics, Tongji University, Shanghai 200092, People's Republic of China
E-mail: shj@nuaa.edu.cn

Published in Micro & Nano Letters; Received on 20th July 2013; Revised on 23rd August 2013; Accepted on 19th September 2013

Molecular dynamics simulations were performed to investigate the wrinkling deformation of one single-layer graphane (GA) sheet under shear, and the shear deformation was compared with that of the macromembrane under shear. Furthermore, the thermal conductivity of the wrinkled GA sheet at 300 K was calculated. Moreover, the differences of anti-shear capability and thermal conductance between the GA and another corresponding graphene sheet are discussed. The results show that the solutions of the macromembrane are applicable to predict the wrinkling deformation of the GA sheet under shear and that both the GA and the graphene sheet under shear have comparable anti-buckling capability, whereas the GA sheet has much lower post-buckling load-carrying capacity. By increasing the shear strain, the thermal conductivity of both the GA and the graphene sheets decreases, and under the same shear strain the graphene sheet has higher thermal conductivity than the GA sheet.

1. Introduction: Carbon nanomaterials have been intensively investigated in recent decades. In spite of the large amount of experimental and theoretical reports, the discovery of new carbon structures seems endless, the carbon nanotube and fullerene being recent examples. Nowadays, graphene is one of the most important subjects in carbon materials science [1–5]; its special two-dimensional (2D) structure of sp^2 carbon atoms results in its very unusual electronic and mechanical properties [6–10].

Graphane (GA), a new graphene derivative, is a quasi-2D covalently bonded hydrocarbon. It was first predicted by Sluiter and Kawazoe [11] in 2003 and discovered by Sofo *et al.* [12] in 2007. GA has two most stable conformations: a chairlike conformer with the hydrogen atoms alternating on both sides of the plane and a boatlike conformer with the hydrogen atoms alternating in pairs [12]. Owing to the potential applications of GA in the fields of astronomy, nuclear industries, nanomaterials and electronic components [13–18], recently a lot of experimental and theoretical investigations have been performed on the electronic and thermal properties of hydrogenated graphene, that is, GA [19–22]. These insights can help us predict the electronic properties of GA-based devices [19–22], as well as the lattice thermal properties of GA such as thermal contraction and heat capacity [23].

The electronic and thermal properties of graphene sheets will change because of deformation under external force [24, 25]. How about GA, hydrogenated graphene? We did not find any report on GA wrinkling under shear, as well as the effect of wrinkling deformation on its thermal conductivity. In this work, we simulated a rectangular chairlike GA sheet under shear using the Tersoff-potential-based MD (molecular dynamics) method, and compared the anti-shear capability of the GA sheet with that of a corresponding graphene sheet, as well as the wrinkling deformation of the GA sheet with that of the macromembrane under shear. Then, EMD (equilibrium molecular dynamics) simulations with periodic boundary conditions were performed to study the thermal conductivity of the wrinkled GA sheet at room temperature. Some results given in this Letter may be helpful for further utilisation of GA.

2. Methodology: Fig. 1 shows our investigated object, a rectangular single-layer GA sheet; its width W is about 5.4 nm, and its length L about 13 nm. The GA sheet is chairlike, and has 2640 carbon atoms and 2640 hydrogen atoms; its C–C bonds are about 0.158 nm long [26]. For clarity, an X – Y coordinate system is established in Fig. 1.

The MD method was used to simulate the shear of the GA sheet. In the simulation, the leftmost line of the atoms in Fig. 1a was ‘fixed’, and shear displacement was exerted on the rightmost line. The loading-rate of 0.03 nm per 1000 time-steps, the time-step of 0.5 fs and the NTV (constant-particle number/constant-temperature/constant-volume) ensemble were taken; Nose’s thermostat [27] was used to control temperature at 300 K (room temperature); periodic boundary condition was applied in the Y -direction. Before the MD simulation, both the leftmost and rightmost lines of atoms in the GA sheet were fixed, and the other atoms were relaxed for 200 000 time-steps at 300 K via the MD method.

After configuration of the GA sheet under certain shear strain was obtained through the above method, the GA sheet was ‘put’ into one 5.4×13 nm cell with periodic boundary condition in both the X - and Y -directions, and its thermal conductivity in the Y -direction was further calculated by the MD method.

In classical MD simulation, the atoms are regarded as basic particles, and the temperature of the simulated molecular system is given through the equipartition theorem of energy. When the practical temperature is much lower than the Debye temperature of the material, the thermal capacity will be highly correlative with the temperature of the system, the equipartition theorem of energy will become invalidated [28] and the quantum correction to temperature needs to be performed. In the present MD calculations of thermal conductivity, the temperature T was taken as the room temperature (300 K), hence, the quantum effects were ignored.

In our present MD simulations, the Velocity-Verlet algorithm was taken, and the Tersoff potential, one three-body potential based on the concept of bond order, was used to describe the interaction between atoms. The Tersoff potential is a famous many-body potential; it explicitly includes an angular contribution of the force and has been widely used to simulate carbon–hydrogen systems [29]. For the interactions between two neighbouring atoms i and j , the energy Φ for the Tersoff potential has the following form

$$\Phi = \sum_i \sum_{j>i} f_c [a_{ij} \cdot E_r(r_{ij}) - b_{ij} \cdot E_a(r_{ij})] \quad (1a)$$

with

$$\begin{aligned} E_r(r_{ij}) &= A_{ij} \cdot \exp(-\lambda_{ij} \cdot r_{ij}) \\ E_a(r_{ij}) &= B_{ij} \cdot \exp(-\mu_{ij} \cdot r_{ij}) \end{aligned} \quad (1b)$$

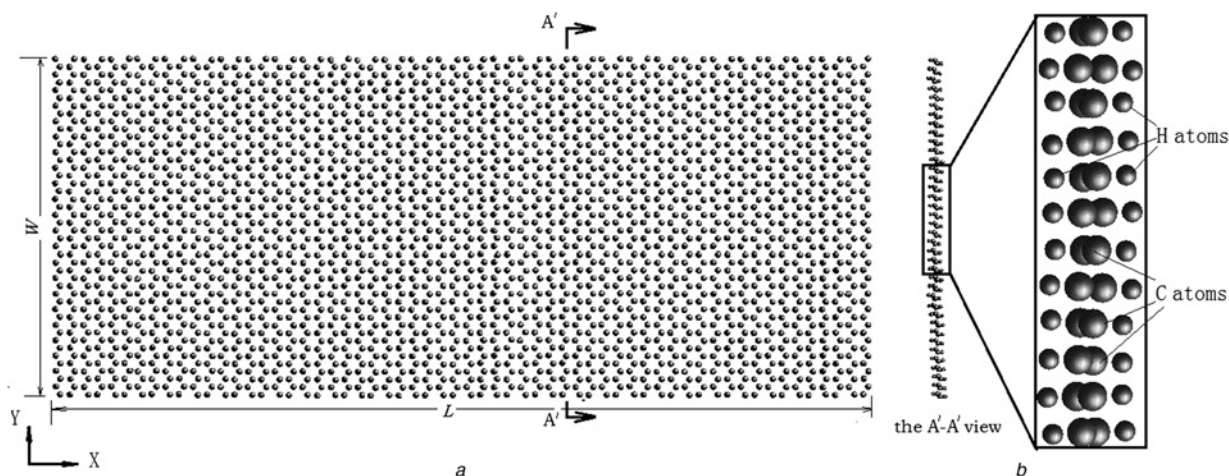


Figure 1 Single-layer GA sheet

a Front view
b Side view

$$f_c(r_{ij}) = \begin{cases} 1 & r_{ij} < R_{ij} \\ 1/2 \left[1 + \cos\left(\pi \frac{r_{ij} - R_{ij}}{S_{ij} - R_{ij}}\right) \right] & R_{ij} < r_{ij} < S_{ij} \\ 0 & S_{ij} < r_{ij} \end{cases} \quad (1c)$$

where the indices i and j run over the atoms of the system, and r_{ij} is the distance from atom i to atom j ; the function E_r represents a repulsive pair potential and E_a represents an attractive pair potential associated with bonding. F_c is a smooth cutoff function, to limit the range of the potential, since for many applications short-ranged functions permit a tremendous reduction in computational effort; b_{ij} is the many-body order parameter describing how the bond-formation energy is affected by the local atomic arrangement because of the presence of other neighbouring atoms (the k -atoms). b_{ij} is a many-body function of the positions of the atoms i , j and k , and has the form of

$$b_{ij} = \chi_{ij}(1 + \beta_i^{n_i} \cdot \xi_{ij}^{n_i})^{-m_i/2n_i} \quad (2a)$$

with

$$\xi_{ij} = \sum_{k \neq i, j} f_c(r_{ik}) \omega_{ik} \cdot g(\theta_{ijk}) \quad (2b)$$

$$g(\theta_{ijk}) = 1 + \frac{c_i^2}{d_i^2} - \frac{c_i^2}{d_i^2 + (h_i + \cos \theta_{ijk})^2} \quad (2c)$$

$$\alpha_{ij} = \varepsilon_{ij}(1 + \beta_i^{n_i} \cdot \tau_{ij}^{n_i})^{-1/2n_i} \quad (2d)$$

where r_{ij} is the distance of the i th and j th atom, θ_{ijk} is the angle between r_{ij} and r_{jk} , $g(\theta_{ijk})$ is a factor considering the angle θ_{ijk} , and $f_c(r_{ij})$ is a truncation function. A_i , B_i , k_i , l_i , e_{ij} , v_{ij} , b_i , n_i , m_i , d_{ik} , x_{ik} , c_i , d_i , h_i , R_{ij} and S_{ij} are some correlative constants with the C, C-H or H system [29, 30].

In our EMD simulations to calculate the thermal conductivity of the GA sheet, based on the Green-Kubo linear response theory, the thermal conductivity λ can be determined according to the following formula [31]

$$\lambda = \frac{1}{K_B T^2 V} \int_0^{+\infty} \langle q(t) \cdot q(0) \rangle dt \quad (3)$$

where K_B is the Boltzmann constant, T is the simulative temperature, $V = d \times W \times L$, where the thickness d of the GA layer takes 0.113 nm [32] as the volume of the simulated system, t is time and q the effective heat flux.

The effective heat flux q can be calculated by the following expression [31]

$$q(t) = \sum_i v_i e_i + \sum_i r_i \frac{de_i}{dt} \quad (4)$$

where v_i is the velocity of the i th atom, e_i is the total energy of the i th atom and r_i is the coordinate.

In [33, 34], we developed a Tersoff-potential-based MD code, and discussed the validity of the code. In recent literature, the code has been widely used to investigate the mechanical and thermal properties of carbon nanomaterials, for example carbon nanotubes [33], graphene [35], fullerenes [36, 37] and nanopeapods [38]. In the present Letter, the MD code was used again.

3. Results and discussion

3.1. Wrinkling deformation of GA sheet under shear: Fig. 2 presents the molecular configurations of the GA sheet under different shear strain ε ; Fig. 3 shows the change of shear stream Q with ε . Here, ε is defined as shear displacement divided by the length L of the GA sheet, and Q as shear force divided by the width W .

Some results can be obtained from Figs. 2 and 3:

1. With the increase of ε , Q increases zigzag; when ε reaches ε_c (≈ 0.43), Q decreases sharply with increasing ε . Our simulations show that when ε reaches about 0.43, the GA sheet cracks at one loading end (see Fig. 2d), and the local stress energy releases suddenly so that Q decreases sharply. Here, ε_c is defined as ‘cracking strain’, and the shear stream Q_c , corresponding to ε_c in the $Q - \varepsilon$ curve, as ‘cracking shear stream’, respectively.
2. In the $Q - \varepsilon$ curve of the GA sheet, the arrow \downarrow marks a big fluctuation, and the fluctuation corresponds to the shear strain ε_f about 0.064 and the shear stream Q_f about 7.9 N/m. Our observations show that when $\varepsilon < \varepsilon_f$, the wrinkles in the GA sheet are very slight, and that when $\varepsilon > \varepsilon_f$, the wrinkles become obvious, that is to say, the sheared GA sheet has buckled. Here, the ε_f and Q_f are defined as ‘buckling shear strain’ and ‘buckling shear stream’, respectively.
3. After buckling of the GA sheet, several out-of-plane wrinkles appear at an approximately 45° angle to the shear boundary

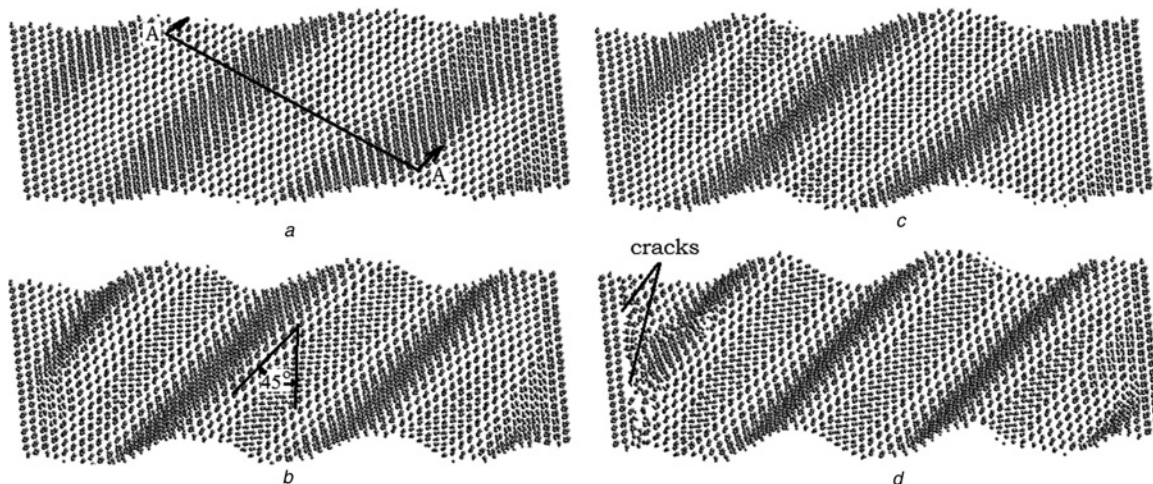


Figure 2 Wrinkling of the GA sheet under shear strain ε

a $\varepsilon = 0.19$

b $\varepsilon = 0.28$

c $\varepsilon = 0.37$

d $\varepsilon = 0.46$

(see Fig. 2b); with the increase of shear strain ε , the out-of-plane amplitude A of the wrinkles increases, and the wavelength (the gap between the wrinkles) decreases. This phenomenon is very similar to the shear buckling of the macromembrane [39–42], and can be explained by using the classical tension field theory of macromechanics [39].

In Fig. 3, another $Q-\varepsilon$ curve, calculated by us, for a rectangular graphene sheet is also presented. Here, the graphene sheet is also chairlike; its width W is about 6 nm, and the length L about 14 nm. By comparing the two $Q-\varepsilon$ curves, we find that:

1. ε_f and Q_f of the graphene sheet are about 7.9 N/m and 0.064, respectively; they also correspond to a big fluctuation, marked with the arrow ‘→’, in the $Q-\varepsilon$ curve of the graphene sheet. The values are close to those of the GA sheet, 8.1 N/m and 0.061, respectively. This implies that both the GA sheet and the graphene sheet under shear have comparable anti-buckling capability.
2. When $\varepsilon > \varepsilon_f$, both the GA and the graphene sheet enter post-buckling state. During the state, under the same ε the shear stream Q of the graphene sheet is obviously larger than that of the GA sheet. ε_c and Q_c of the graphene sheet are about 0.53 and 33.0 N/m, respectively, corresponding to the point marked with

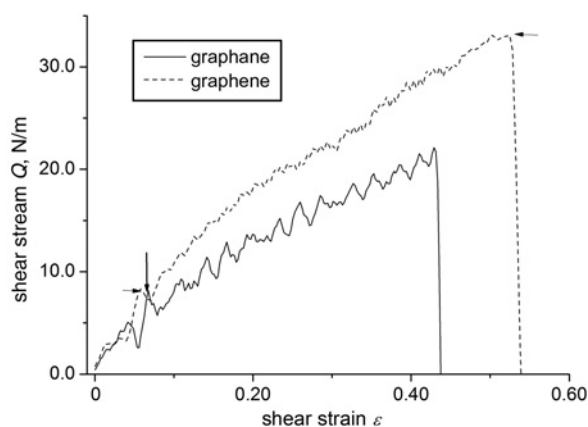


Figure 3 $Q-\varepsilon$ (shear stream against shear strain) curves of the GA and graphene sheets

the arrow ‘←’ in the $Q-\varepsilon$ curve of the graphene sheet; the ε_c and Q_c values are much larger than those of the GA sheet, 0.43 and 21.6 N/m, respectively. All these imply that the GA sheet has much lower post-buckling load-carrying capacity than the graphene sheet.

To further study the configuration of the wrinkled GA sheet, Fig. 4 shows a local cross-section of the wrinkles, that is, the A-A cross-section in Fig. 2a. The local cross-section, perpendicular to the direction of the wrinkles, is relatively far away from the two shear boundaries so as to reduce the edge effects. For argument’s sake, an $\xi-w$ coordinate system is established in Fig. 4. It is obvious that the cross-section of the wrinkles can be approximately described with the help of sinusoidal functions

$$w = A \cdot \sin(\pi\xi/\eta) \quad (5a)$$

where w is the out-of-plane displacement, A is the out-of-plane amplitude of the wrinkles and η is the half wavelength of the wrinkles (the half gap between the wrinkles).

Fig. 5 presents the $A-\varepsilon$ and $\eta-\varepsilon$ data for the present MD simulations.

Wong and Pellegrino [39–41] gave the cross-section formula of the wrinkles in sheared membrane through experiment and numerical simulation. Wong’s formula has the same form as (5a). In the formula

$$\eta = \frac{\sqrt{\pi}}{[3(1-\nu^2)]^{1/4}} \frac{\sqrt{Wd}}{\varepsilon^{1/4}} \quad (5b)$$

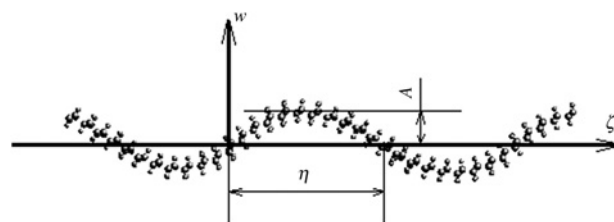


Figure 4 Cross-section of wrinkles, that is the A-A cross-section of Fig. 2a

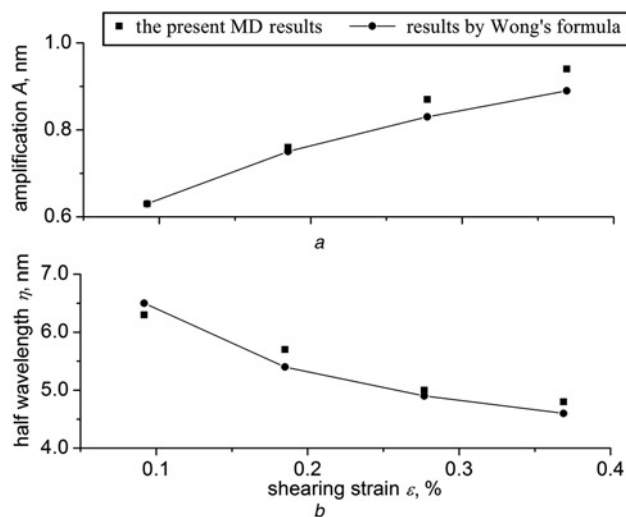


Figure 5 *A* – ϵ and η – ϵ curves for the sheared GA sheet
a *A* – ϵ
b η – ϵ

and

$$A = \frac{\sqrt{2(1-\nu)}}{\sqrt{\pi[3(1-\nu^2)]^{1/4}}} \sqrt{Wd} \cdot \epsilon^{1/4} \quad (5c)$$

where ν is the Poisson's ratio of the membrane.

Wong's formula is about the macromembrane. Is it suitable for the present GA sheet? We used Wong's formula to predict the GA sheet, and the predicted *A* – ϵ and η – ϵ results are also shown in Fig. 5. In [26], the given Poisson's ratio ν of the GA sheets is 0.392–0.675; in the prediction ν takes the middle value 0.54.

From Fig. 5, we find that the predicted *A* – ϵ and η – ϵ results through Wong's formula are close to the present MD results, which implies that Wong's expression is suitable for prediction of the GA sheets wrinkling under shear.

3.2. Thermal conductivity of the wrinkled GA sheet: Previous studies showed that the contribution to thermal conductivity of nanomaterial mainly comes from two factors [35]. The first one is the interaction between electrons and phonons, and the second one is the interaction between phonons. The former is dependent on molecular configuration (electronic structures) and phonon scattering; the latter is correlative to atomic vibration.

Fig. 6 presents the change of thermal conductivity λ of the GA sheet with shear strain ϵ . In the Figure, the λ – ϵ curve of the graphene sheet mentioned in Section 3.1 is also given. Here, the temperature takes 300 K, and the thickness *d* of the graphene sheet takes 0.144 nm [42]. According to Fig. 6 and our simulations we find that

1. With the increase of shear strain ϵ , the deformation of both the GA and the graphene sheet becomes more serious, and therefore, their thermal conductivity λ decreases. The following reasons can be used to explain this phenomenon. Firstly, shear strain causes the deformation of the GA and graphene sheets; and undulates the heat transfer path, which results in the increase of phonon scattering. Secondly, under shear, the C–C chemical bonds in both the GA and the graphene sheet are in tension or compression; the larger the shear strain, the tighter the tension or compression on the C–C bonds, which will cause slight change in the lattice vibration mode, that is, the change in vibration-frequency and amplitude, as well as the decrease in thermal conductivity.

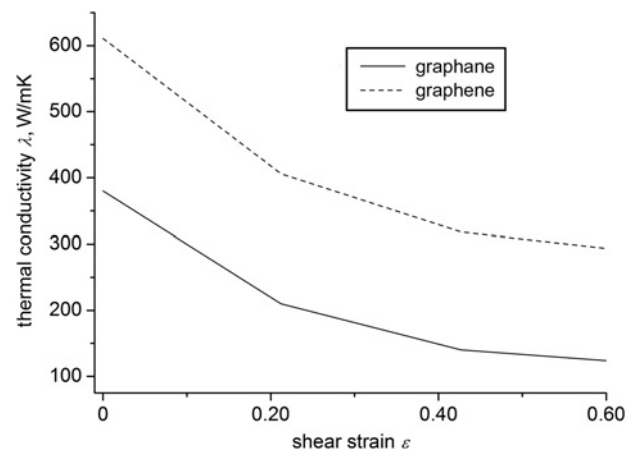


Figure 6 Thermal conductivity λ of the GA and graphene sheets under shear strain ϵ

2. Under the same shear strain, the GA sheet has much lower thermal conductivity than the graphene sheet, which mainly results from their difference in molecular configuration. One ideal graphene sheet with the C–C bonds of the sp^2 structure is approximately planar; this allows the phonons to transfer in the graphene plane. By contrast, the C–C bonds of one ideal GA sheet have the sp^3 structure, and are not in one plane (see Fig. 1b), hence, the GA sheet has more phonons scattering than the graphene sheet.

4. Conclusions: The Tersoff-potential-based MD method was applied to simulate the shear wrinkling of a GA sheet, and the obtained wrinkling deformation was compared with Wong's analytical solution of the macromembrane under shear. Furthermore, the thermal conductivity of the GA sheet was calculated. The mechanical properties and thermal conductivity of the GA sheet under shear were also compared with those of a graphene sheet, respectively. The following main conclusions were obtained:

1. When the shear strain ϵ reaches ϵ_f (≈ 0.064), the GA sheet buckles, and when ϵ reaches 0.43, the GA sheet cracks. The present MD results about the wrinkling deformation of the GA sheet under shear are consistent with Wong's expression about the macromembrane; that is, Wong's expression is able to predict the wrinkles of the GA sheets under shear. The GA sheet under shear has comparable anti-buckling capability with the graphene sheet, but much lower post-buckling load-carrying capacity than the graphene sheet.
2. With the increase of shear-deformation, the thermal conductance of the GA sheets and graphene sheets becomes worse. Under the same shear strain, the GA sheet has much lower thermal conductivity than the graphene sheet.

5. Acknowledgment: This work was supported by the Natural Science Foundation of Shanghai (no. 13ZR1444000).

6 References

- [1] Novoselov K.S., Geim A.K., Morozov S.V.: 'Electric field in atomically thin films', *Science*, 2004, **306**, (5696), pp. 666–669
- [2] Van den Brink J.: 'Graphene: from strength to strength', *Nature Nanotechnol.*, 2007, **2**, (4), pp. 199–201
- [3] Geim A.K., Novoselov K.S.: 'The rise of graphene', *Nature Mater.*, 2007, **6**, (3), pp. 183–191
- [4] Avouris P., Chen Z., Perebeinos V.: 'Carbon-based electronics', *Nature Nanotechnol.*, 2007, **2**, (10), pp. 605–615
- [5] Yue C., Hill J.: 'Modelling interaction of atoms and ions with graphene', *Micro Nano Lett.*, 2010, **5**, (5), pp. 247–250

- [6] Lee C., Wei X., Kysar J.W.: 'Measurement of the elastic properties and intrinsic strength of monolayer graphene', *Science*, 2008, **321**, (5887), pp. 385–388
- [7] Grantab R., Shenoy V.B., Ruoff R.S.: 'Anomalous strength characteristics of tilt grain boundaries in graphene', *Science*, 2010, **330**, (6006), pp. 946–948
- [8] Balandin A.A., Ghosh S., Bao W.: 'Superior thermal conductivity of single-layer graphene', *Nano Lett.*, 2008, **8**, (3), pp. 902–907
- [9] Kim K., Lee Z., Malone B.D.: 'Multiply folded graphene', *Phys. Rev. B*, 2011, **83**, p. 245433
- [10] Hu Z., Chen Y., Hou Q., Yin R., Liu F., Chen H.: 'Characterization of graphite oxide after heat treatment', *New J. Chem.*, 2012, **36**, pp. 1373–1377
- [11] Sluiter M., Kawazoe Y.: 'Cluster expansion method for adsorption: application to hydrogen chemisorption on graphene', *Phys. Rev. B*, 2003, **68**, p. 085410
- [12] Sofo J.O., Chaudhari A.S., Barber G.D.: 'Graphane: a two-dimensional hydrocarbon', *Phys. Rev. B*, 2007, **75**, p. 153401
- [13] Baughman R., Galvao D., Cui C., Wang Y.: 'Fullerenynes – a new family of porous fullerenes', *Chem. Phys. Lett.*, 1993, **204**, pp. 8–14
- [14] Coluci V., Braga S., Legoas S., Baughman R.: 'Graphyne-based nanotubes', *Phys. Rev. B*, 2003, **68**, p. 035430
- [15] Huang L., Ni M., Zhang G.: 'Modulation of the thermodynamic, kinetic and magnetic properties of the hydrogen monomer on graphene by charge doping', *J. Chem. Phys.*, 2011, **135**, p. 3624657
- [16] Areou E., Cartry G., Layet J., Angot T.: 'Hydrogen-graphite interaction: experimental evidences of an adsorption barrier', *J. Chem. Phys.*, 2011, **134**, p. 14701
- [17] Flores M., Autreto P., Legoas S., Galvao D.: 'Graphene to graphane: a theoretical study', *Nanotechnology*, 2009, **20**, (46), p. 5704
- [18] Huang L., Li Y., Ni M.: 'Lattice dynamics of hydrogen-substituted graphene systems', *Acta Phys. Sin.*, 2009, **58**, pp. 306–312
- [19] Karssemeijer L., Fasolino A.: 'Phonons of graphene and graphitic materials derived from the empirical potential LCBOP-II', *Surf. Sci.*, 2011, **605**, pp. 1611–1615
- [20] Tewary V., Yang B.: 'Singular behaviour of the Debye-Waller factor of graphene', *Phys. Rev. B*, 2009, **79**, p. 125416
- [21] Bang J., Chang K.: 'Localization and one-parameter scaling in hydrogenated graphene', *Phys. Rev. B*, 2010, **81**, p. 193412
- [22] Soriano D., Munoz-Rojas F., Fernandez R.: 'Hydrogenated graphene nanoribbons for spintronics', *Phys. Rev. B*, 2010, **81**, p. 165409
- [23] Neek-Amal M., Peeters F.: 'Lattice thermal properties of graphane: thermal contraction, roughness and heat capacity', *Phys. Rev. B*, 2011, **83**, p. 235437
- [24] Bao W., Miao F., Chen Z., Zhang H., Jang W.: 'Controlled ripple texturing of suspended graphene and ultrathin graphite membranes', *Nature Nanotechnol.*, 2009, **4**, pp. 562–566
- [25] Kim Z., Lee Z., Malone B.: 'Multiply folded graphene', *Phys. Rev. B*, 2011, **83**, p. 245433
- [26] Scarpa F., Chowdhury R., Adhikari S.: 'Thickness and in-plane elasticity of graphane', *Phys. Lett. A*, 2011, **375**, pp. 2071–2074
- [27] Nose S.: 'A unified formulation of the constant temperature molecular dynamics method', *J. Chem. Phys.*, 1984, **81**, pp. 511–519
- [28] Tian S., Shen H.: 'Thermal and tensile properties of BN, SiC and Ge nanotubes', *J. Mater. Eng. Sci.*, 2008, **26**, (6), pp. 135–139
- [29] Tersoff J.: 'Empirical interatomic potential for carbon, with applications to amorphous carbon', *Phys. Rev. Lett.*, 1988, **61**, (25), pp. 2879–2882
- [30] Tersoff J.: 'Modeling solid-state chemistry: interatomic potentials for multicomponent systems', *Phys. Rev. B*, 1989, **39**, p. 5566
- [31] Irving J., Kirkwood J.: 'The statistical mechanical theory of transport processes. IV: the equations of hydrodynamics', *J. Chem. Phys.*, 1950, **18**, (6), pp. 817–829
- [32] Elias D., Nair R., Mohiuddin T., *ET AL.*: 'Control of graphene's properties by reversible hydrogenation: evidence for graphane', *Science*, 2009, **323**, (5914), pp. 610–613
- [33] Shen H.: 'MD simulations on the melting and compression of C, SiC and Si nanotubes', *J. Mater. Sci.*, 2007, **42**, (15), pp. 6382–6387
- [34] Shen H.: 'Thermal-stability and tensile properties of two single-walled Si-H nanotubes', *Mol. Simul.*, 2007, **33**, (11), pp. 939–944
- [35] Shen H., Chen K.: 'Tensile properties and thermal conductivity of graphene nanoribbons encapsulated in single-walled carbon nanotube', *Mol. Simul.*, 2012, **38**, (11), pp. 922–927
- [36] Shen H.: 'Mechanical properties and electronic structure of compressed C₆₀, C₁₈₀ and C₆₀@C₁₈₀ fullerenes', *J. Mater. Sci.*, 2007, **42**, (17), pp. 7337–7342
- [37] Shen H.: 'Collision and energy transfer between C₆₀ fullerenes in one Ar atoms filled carbon nanopeapod', *Nano*, 2007, **2**, (1), pp. 35–39
- [38] Shen H.: 'Compressive and tensile mechanical properties of Ar-filled carbon nanopeapods', *Mater. Lett.*, 2007, **61**, (2), pp. 527–531
- [39] Wong Y., Pellegrino S.: 'Wrinkled membranes III: numerical simulations', *J. Mech. Mater. Struct.*, 2006, **1**, (1), pp. 63–96
- [40] Wong Y., Pellegrino S.: 'Wrinkled membranes I: experiments', *J. Mech. Mater. Struct.*, 2006, **1**, (1), pp. 1–20
- [41] Wong Y., Pellegrino S.: 'Wrinkled membranes II: analytical models', *J. Mech. Mater. Struct.*, 2006, **1**, (1), pp. 25–59
- [42] Guo Z., Zhang D., Gong X.: 'Thermal conductivity of graphene nanoribbons', *Appl. Phys. Lett.*, 2009, **95**, p. 163103